Electric Field Measurements and Calculations for the STAR FTPC

H. Hümmler

Max-Planck-Institut für Physik, München, Germany

Abstract

This STAR note will give an overview of certain principal hardware matters that were of some concern in the course of the development of the STAR FTPCs and that did not evolve into parts of the data reconstruction software. After a short introduction into the design basics of the FTPC, chapter 2 will briefly summarize the studies on special problems of a radial drift TPC done by Marstaller [Mar98]. The following chapters describe special calculations on the distortions in the detector's electric field configuration, which were done to verify the design of certain FTPC components before the start of production.

This STAR note is based on parts of Holm Hümmler's Ph.D. thesis. The full text of the thesis is available from http://wwwstar.mppmu.mpg.de/Doc/hh_thesis.ps.gz

Chapter 1

Introduction

The main part of the STAR detector was designed for optimum performance around midrapidity, in a rapidity range from -1.5 to $+1.5$. However, this acceptance covers only about 50% of the particles expected to be produced in a heavy ion collision at RHIC. With slight variations depending on the model, about 30% of the particles produced are expected in a pseudorapidity range of $2.5 <| \eta |< 4.0$ [Bie98]. A tracking detector in this region can offer important data for the analysis of several observables, like baryon stopping, flow and the search for disoriented chiral condensates.

The cylindrical Forward Time Projection Chambers (FTPCs) were built for this role in the STAR experiment. Besides physics specifications and financial limits, their design was strongly influenced by spatial constraints:

- The cylindrical free space inside the central TPC, where the FTPCs are located, limits their outer radius to 35 centimeters including the front-end electronics and cooling.
- Sufficient thermal and electromagnetic decoupling from the aluminum pipe surrounding the circulating ion beam demands an inner radius of at least 7.5 centimeters.
- To limit the radiation background in the central TPC, no solid matter could be introduced within 150 cm in beam direction from the main interaction point.
- Because of the divergence of the magnetic field beyond a distance of 270 cm in beam direction from the interaction point, extending the sensitive area beyond this distance would not have significantly improved the momentum resolution.
- There is only one stable structure for suspension available: the central TPC support frame, which is about 220 cm in beam direction from the main interaction point.

On the physics side, the primary task of the FTPC, to determine the charge and momentum of charged hadrons emitted within its acceptance, faces a number of challenges. They mostly result from the fact that the particles studied are emitted at small angles to the beamline:

- The particle trajectories have small angles to the beam direction. Therefore, to achieve a reasonable position resolution, the drift direction of the FTPC could not be parallel to the beam (as in the case of the central TPC), but radial onto the outer surface of the cylinder.

- As the detector is located in a solenoid magnet, the particle trajectories are almost parallel to the magnetic field lines. Therefore, the Lorentz force

$$\vec{F} = q(\vec{v} \times \vec{B}) \tag{1.1}$$

  is small compared to the total momentum. A transverse momentum of 1 GeV/c corresponds to a radius of 7 m in the x/y-projection, in which the track is only about 20 cm long. To get reasonable accuracy in determining the charge and momentum of the particles, the position resolution of the detector at the individual track points has to be:

$$\sigma \leq 150\,\mu m \tag{1.2}$$

- Between the main interaction point and the sensitive volume of the detector, the particles have to pass through the material of the beampipe, beampipe support and the inner parts of the FTPC. Processes relevant for the measurement of hadrons include electromagnetic multiple scattering as well as hard interactions with the nuclei in the traversed matter. Also, conversion of gamma rays to electron-positron pairs is one of the major sources of background in the measurement.

- The density of charged particle tracks in the acceptance of the FTPC is extremely high. The sensitive cross-section of one FTPC of only $0.25\,\mathrm{m}^2$ is traversed by more than 500 charged hadrons in each interaction. This track density even increases for small radii. Therefore, the detector must have a good capability to discern parallel tracks at small distances (two-track separation).

The relative contributions of these influences to the momentum resolution achievable with the detector will be discussed in STAR note 430.

The design of the FTPCs is shown in figure 1.1. They are designed as TPCs with a radial drift field, with readout chambers located on the cylindrical outer surface, at a radius of 31 cm. The high voltage electrode of each FTPC is a thin tube surrounding the beampipe, made of plastic material which has been galvanically coated with metal to define a cylindrical surface of constant negative potential, at a radius of 8 cm. The field cage to close the field at both ends of the cylinder consists of concentric rings made from aluminum pipes with a wall thickness of only 300 μm. The main support structure for each FTPC has been milled out of one single tube of aluminum, to provide the necessary precision and stability. The support frame and the installed readout chambers form a gas tight cylindrical surface. At both ends of the cylinder, the gas volume is closed off by a double window made of aluminized mylar foil.

The frontend electronics, which preamplifies, shapes and digitizes the signals is installed on the back of the readout chambers. To limit the number of electronics channels without increasing the pad pitch, the number of padrows was limited to ten per FTPC. Therefore, the padrows are not adjacent, and the particle tracks are only sampled about once in ten centimeters. Each circular padrow has 960 pads.

The readout plane of one FTPC is segmented into 30 readout chambers, which can be individually disconnected from the support frame for maintenance. Each readout chamber holds two padrows on 1/6 of the circumference of the FTPC. The pads are parallel to the axis of the cylinder (z-direction) and therefore almost parallel to the majority of the produced tracks. The anode wires are mounted on the readout chambers and fixed around each single padrow with conductive glue. The gating and Frisch grid wires, however, are mounted on the main support structure and fixed at both ends of the cylinder.

To achieve a high position accuracy and good two-track separation, the structures in the readout chambers are kept relatively small. The pads are 20 mm long and only 1.6 mm wide, with a pitch of 1.9 mm, and the anode wires are 1.5 mm above the pads. Prototype measurements are consistent with what could be expected from these numbers, indicating a pad response function width of slightly less than 1.5 mm and a two-track separation down to track distances of 1.0 mm at small radii [Sch99].

A more detailed description of the FTPC design can be found in the FTPC proposal [Bie98].

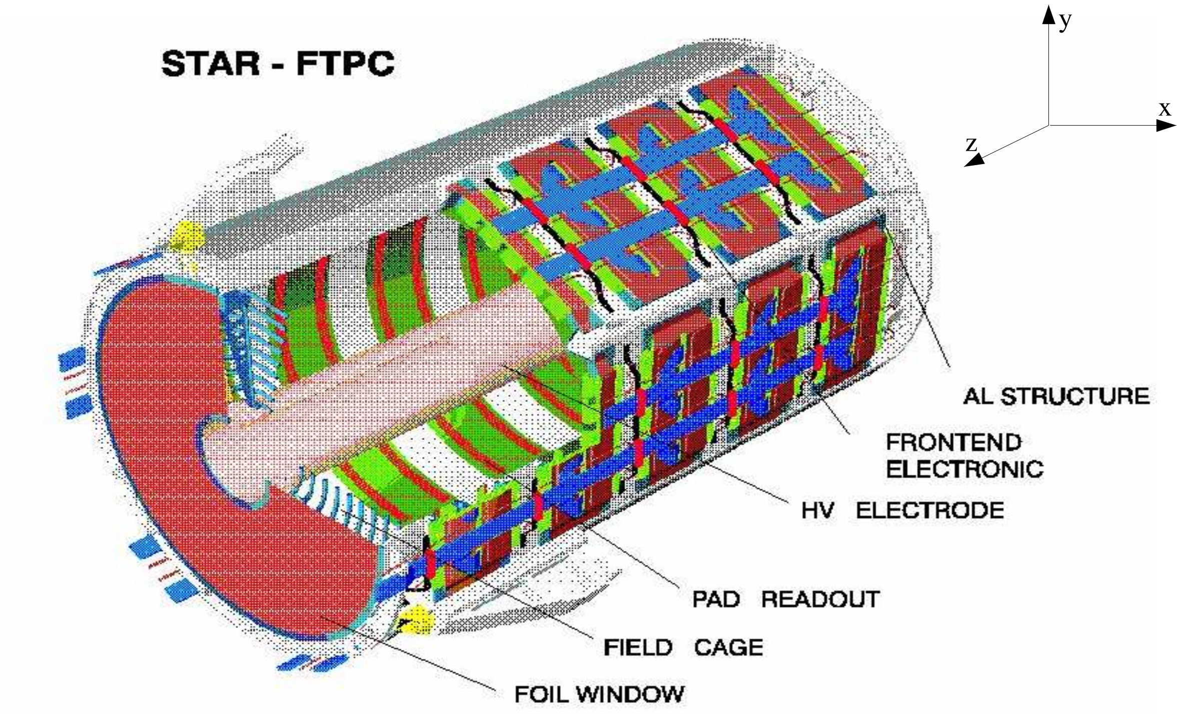

Figure 1.1: *Components of the FTPC design.*

Chapter 2

Problems of a Radial Drift TPC

To achieve a reasonable position resolution, a TPC needs a large angle between particle tracks and drift direction. This, in connection with the cylindrical space available, necessitated a design with a radial drift field. As a further advantage, the radial drift improves the separation of the charge clouds from different tracks, especially for small radii, where the track density is highest [Kon95].

A technical problem posed by the radial drift is the installation of the anode wires. The simple way of installing wires in a cylindrical detector would be in z-direction along the sides of the cylinder, parallel to the pads. If, however, the anode wires are parallel to the pads and, therefore, parallel to the tracks, the charge resulting from each track will be focused to a single anode wire, leading to a quantization of the measured positions and to distortions in the position resolution. Consequently, in conventional TPCs, the anode wires are orthogonal to the pads. In a TPC with a cylindrical readout surface, this is hardly feasible.

One solution, used by the CERES/NA45 experiment, is to split the outer surface of the cylindrical TPC volume into planar segments. This allows simple, planar readout sectors and wires orthogonal to the pads, at the expense of severe distortions in the radial drift field [Bel99].

A different possible solution, intended in early stages of the FTPC planning, is to use micro strip gas chambers (MSGCs) as readout for the TPC. Since their anodes are not wires but metal strips on a glass substrate, they could be bent with the supporting glass and thus be arranged in the ideal direction, orthogonal to the pads. However, test measurements for other experiments have shown stability problems with MSGCs. In hadronic radiation, the small structures were vulnerable to high voltage discharges, which damaged the metal strips. Because development time was short and a robust detector system was needed, the MSGCs were abandoned in favor of a more conventional wire design.

The FTPC readout chamber design uses the fact that the tracks to be measured are almost parallel to the pads and that there is enough space to fix the wires between padrows. If the wires cross the pads at small angles, the plane defined by the wires is still sufficiently parallel to the pad plane. It could be shown that the quantization effect disappears when each pad is crossed by more than one wire, to be seen in figure 2.1 (from [Mar98]). In the FTPC readout chambers, the angle was chosen so that the length of each pad is crossed by exactly three wires, additionally insuring an equal integrated length of anode wire over each pad, as can be seen in figure 2.2.

A further complication caused by the radial drift is that the electric field strength and therefore the velocity of the drifting electrons are not constant. Also, the electric field is not parallel to the magnetic field, but would be perpendicular to the field of a perfect, infinite solenoid. This is complicated even more since the STAR magnet field has some significant inhomogeneities in the volume of the FTPCs. This has to be taken into account and compensated for in the reconstruction of the FTPC data. The resulting code will be discussed in STAR note 429.

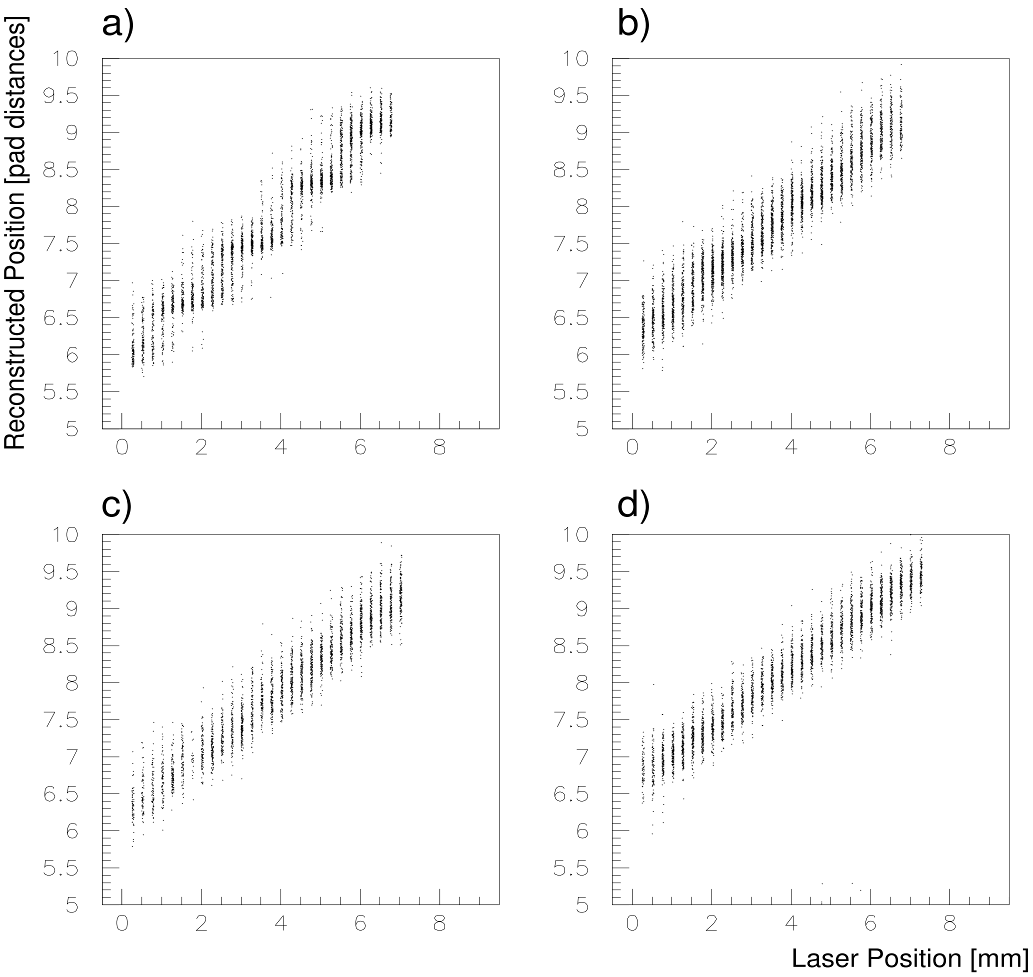

Figure 2.1: *Tests done to find the minimum angle between anode wires and pads by scanning a TPC with laser tracks. The plots show the reconstructed position from the TPC versus the initial laser position. Plot a), with the anode wires parallel to the tracks, shows a quantization structure with the pitch of the anode wires. Plot b), with an angle of 9^o, has no such structure. The reconstruction has similar quality as in plot c), with 16^o and plot d) with 90^o.*

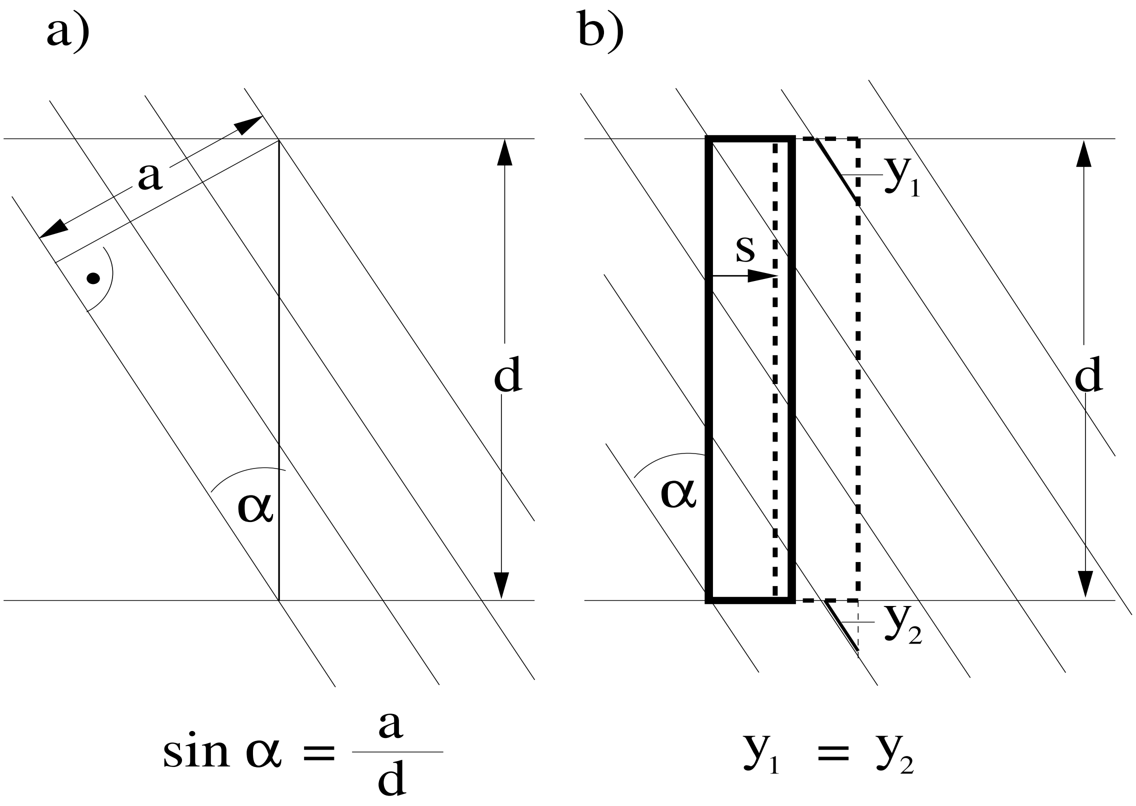

Figure 2.2: *Selection of a favorable angle between the pad direction and the anode wires. Part a) defines the distance a in relation to the pad length d and the angle α between pad direction and anode wires (thin lines). The angle is chosen so that the distance a divided by the pitch of the anode wires is an integer number. Part b) shows that under these conditions the integrated wire length over each pad is identical, as the wire length y_1 added by moving the pad is identical to the subtracted wire length y_2. In the FTPC readout chambers d=20 mm and distance a is three times the wire pitch of 2 mm, so α was set to 17.4^o.*

Chapter 3

The Electric Field in the Readout Region

Ideally, the drift field of a TPC is perfectly homogeneous or radial up to the Frisch grid which separates it from the strongly inhomogeneous but periodic field in the gas amplification volume. In reality, the Frisch grid is never completely intransparent; the gating grid is never completely transparent, and both the drift field and the amplification field are distorted by edge effects of the detector. Distortions in the drift field are usually small, but their effects integrate over the whole path of the drifting electrons. In and around the amplification region, field distortions are usually local but can be of substantial magnitude.

To calculate the distortions close to the amplification region in the FTPCs, a simplified, planar model of a small FTPC segment was calculated using the MAFIA (*Solution of MAxwell's equations using a Finite Integration Algorithm*) electromagnetic simulation package [Bar92]. The effects to be studied were the transparency of the wire grids and the field distortions at the sector edges.

The geometry of the model is shown in figure 3.1. The calculation is done in two dimensions and neglects the cylindrical structure of the FTPC. This approximation is possible because the segment is small compared to the radius of the chamber. The two cartesian coordinates are called R and X because one of them corresponds to the radius in cylindrical FTPC coordinates, the other to the azimuth or to the x-coordinate at the sector boundary around x=0, where the radius would be equivalent to y. The pad plane is simulated by a solid line at ground potential. The anode, Frisch and gating grid wires crossing the model plane are represented by areas corresponding to their cross-sections, set to the respective potentials. The anode wire voltage is set to 1600 V. A solid rectangle of conductive material stands for one strip of conductive glue used to mount the anode wires at the edges of a sector. A solid line set to high voltage simulates the continuation of the drift field, creating a field of $-253\,\mathrm{V/cm}$, the strength of the radial field at the radius of the Frisch grid. The gating grid voltage is calculated assuming a perfectly intransparent Frisch grid.

Insulating materials, like the fiber glass loaded epoxy supporting the conductive glue and the sense wires, are more difficult to include in the model, because their surfaces have unknown potentials. However, experiences in the NA49 experiment indicate that surfaces at undefined potential tend to assume the potential of the surroundings if a sufficient number of positive and negative charges is floating in the chamber gas [Hum97]. In any case, their potential should be between ground and the anode wire voltage; otherwise these surfaces would attract either electrons drifting through the Frisch grid or positive ions drifting away from the anode wires. Therefore, in the model, all insulating materials have been defined as invisible to the electric field and replaced by vacuum.

The resulting potential distribution is shown in Figure 3.2. It also gives a first impression of the distortions introduced by the conductive glue and by the boundary conditions of the model.

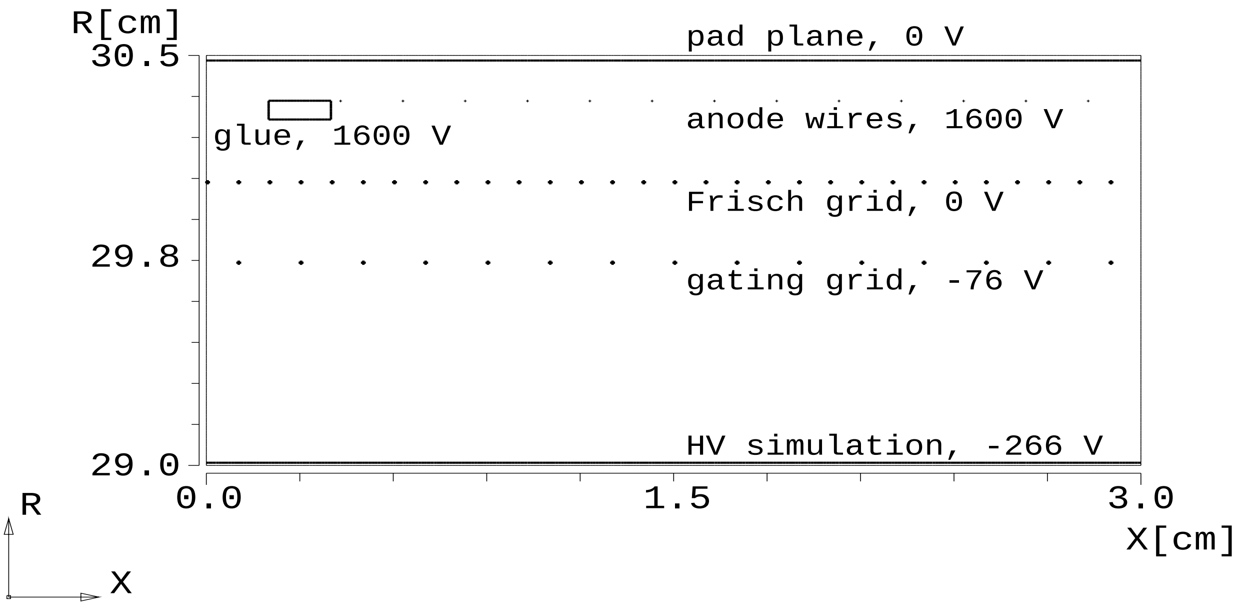

Figure 3.1: *Material distribution in the model to calculate the electric field in the readout region. A solid plate at the top simulates the pad plane. The uppermost line of dots are the anode wires, and the rectangle on the left simulates the strip of conductive glue holding them. The central line of dots stands for the Frisch grid, and the lower line of dots is the gating grid. A solid plate at the bottom of the plot simulates the continuation of the radial drift field.*

3.1 Transparency of the Wire Grids

Figure 3.3 shows the main component of the drift field along a cut in R between the gating grid wires. Ideally, the field should be constant with the calculated magnitude of $-253\,\mathrm{V/cm}$. The curve shows that the field magnitude is slightly larger in the free drift volume, has a step around the gating grid (at $\mathrm{R} = 29.75\,\mathrm{cm}$) and then increases to $-360\,\mathrm{V/cm}$ between the gating grid and the Frisch grid. This is caused by incomplete screening of the amplification field at the Frisch grid. The field of the anode wires reaches through the Frisch grid and the gating grid into the drift volume.

The usual way of trying to compensate for this problem is to introduce a bias voltage on the gating grid. This can be done in two possible ways:

- The gating grid can be adjusted for the best possible transparency, in this case by decreasing the absolute value of its negative voltage by about 30 V. In this case, local disturbances around the gating grid are minimized, but the outer voltage defining the radial field is shifted. Because the field cage is adjusted for the original field configuration, a large-scale three-dimensional distortion of the drift field will result.
- The gating grid can be adjusted to screen the drift field against field leakage through the Frisch grid, in this case by increasing the absolute value of its voltage by about 10 V. In this case, the drift field will be undistorted up to the gating grid, followed by an even larger step and a much higher field strength between the gating grid and the Frisch grid. While this can be interpreted as a gradual transition to the amplification region, it can also lead to systematic distortions in the reconstructed points if it is not properly taken into account in the reconstruction.

The more fundamental approach of compensating for the transparency of the Frisch grid is to apply a bias voltage to the Frisch grid itself. Instead of defining the Frisch grid as made of wires at ground potential, it should be redefined as a plane which is effectively at ground potential, with local disturbances resulting from the wires and the spaces between them. For the voltage configuration described above, the appropriate Frisch grid voltage to get a field without large scale distortions is -43 V.

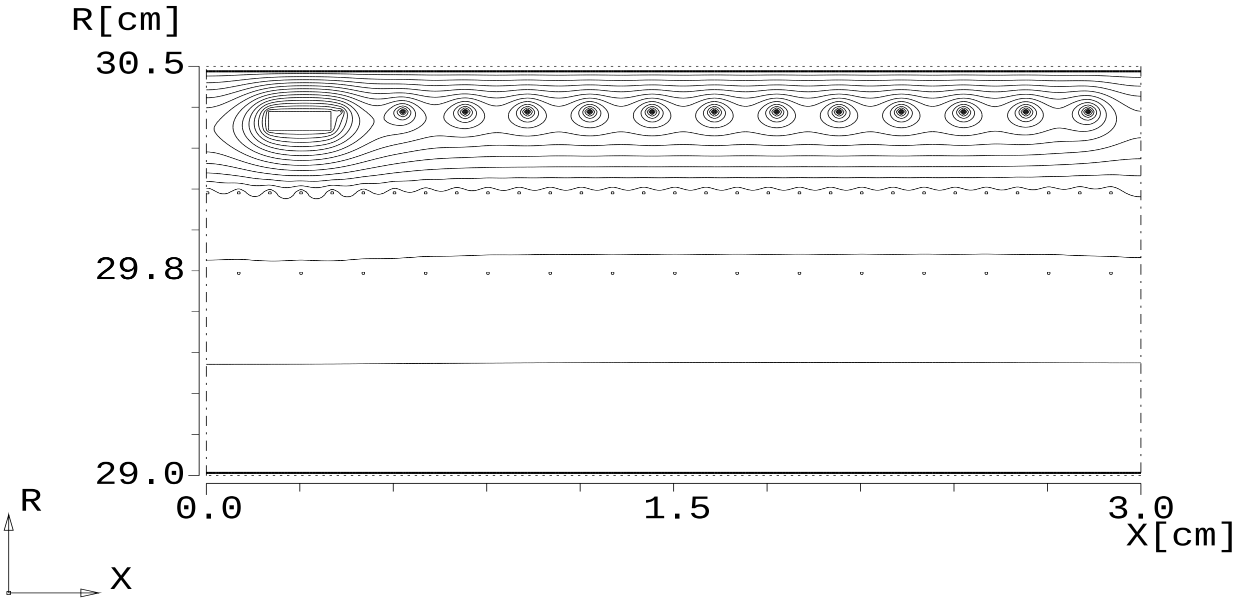

Figure 3.2: *Electric potential distribution in the model. The figure indicates lines of identical potential. High potential gradients indicate the amplification region around the anode wires. The Frisch grid separates the amplification region from the drift field, while the open gating grid should not influence the surrounding potential.*

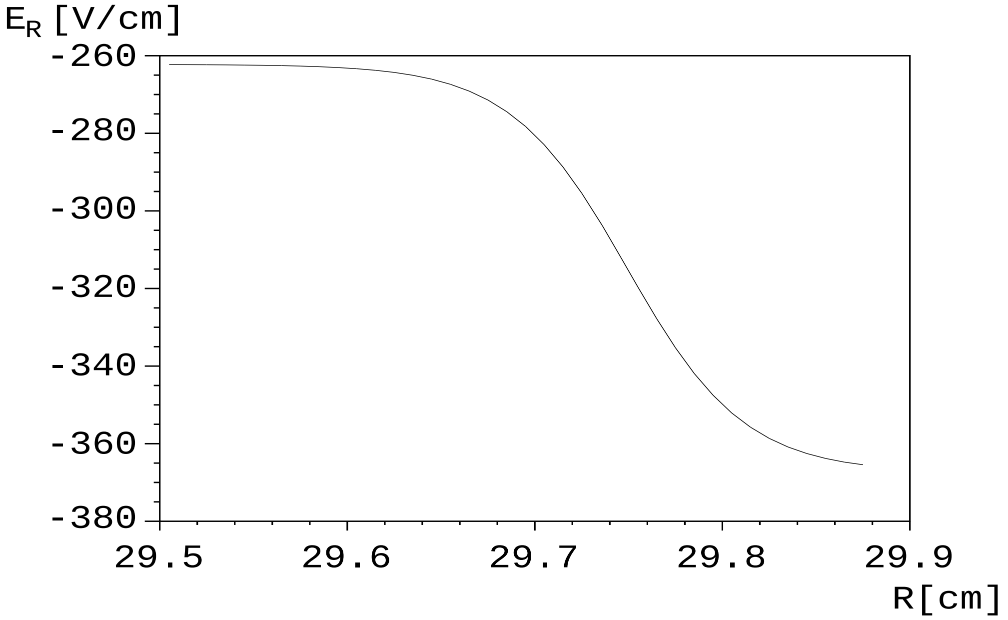

Figure 3.3: *Radial (R) component of the electric field in the drift volume around the gating grid. The cut is at $X = 2.0$ cm, between the wires of the gating grid and ranges from the free drift volume, below 29.6 cm, to the area where local effects from the Frisch grid wires set in, around 29.9 cm.*

3.2 Distortions at the Sector Boundary

The second source of errors to analyze is the sector boundary with the mountings for the sense wires. The conductive glue runs around each padrow, but in the central part of the padrow, each pad is affected equally from both glue lines running along the padrow. At the sector boundaries, however, azimuthal field components from the wire mounting can introduce errors in the azimuthal position resolution. The azimuthal component is the most important for the FTPCs' momentum resolution.

The azimuthal coordinate in the FTPC corresponds to the X coordinate in the MAFIA calculation. Figure 3.4 shows the X component of the electric field in the amplification volume, approximately in the middle between the Frisch grid and the anode wires. On the right, the modulation from the anode wires can be seen. This pattern is connected with the quantization effect discussed in section 2. At small X, towards the sector boundary, the field rises sharply, caused by the positive potential of the conductive glue ranging into the amplification volume. The center of the second pad, the closest point to the sector boundary where a cluster could reasonably be measured, is at $X = 1.0$ cm in the model. At this point, the X component has dropped down to negligible values, so it can be assumed that no significant distortions will be introduced in this region.

The X component of the electric field between the Frisch grid and the gating grid can be seen in figure 3.5. In this region, the total field strength is smaller, so that smaller horizontal components can already have a considerable effect on the electron drift. The X component above the second pad is on the order of 5 V/cm, a 2% effect in the drift field of ideally -253 V/cm. Extrapolating this over the distance of the two grids of 3 mm, a

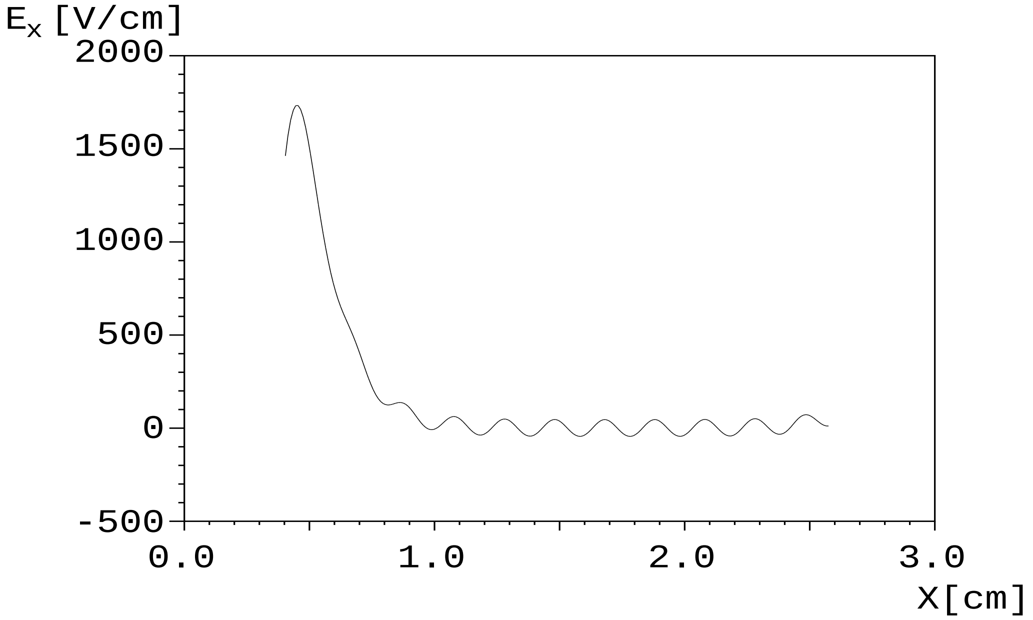

Figure 3.4: *Horizontal (X) component of the electric field between the Frisch grid and the anode grid in the readout region model. The cut is at $R = 30.18\,cm$.*

distortion of about $60\,\mu$m can be expected.

At 1.5 mm below the gating grid, the horizontal component has dropped down to about 2 V/cm (see figure 3.6). Detailed field calculations at larger distances are difficult, because they would have to include the radial field. If a linear dropoff of the horizontal component from the gating grid is assumed, additional distortions of about $30\,\mu$m may be caused by field perturbations below the gating grid.

In total, sector boundary distortions of up to $100\,\mu$m can be expected. These should be visible in a detailed analysis of the deviations of track points from the reconstructed trajectories, so it should be possible to develop correction routines. Because of the few tracks affected and the small magnitude of the effect, however, sector boundary distortions need not be a primary concern in the early stages of the analysis.

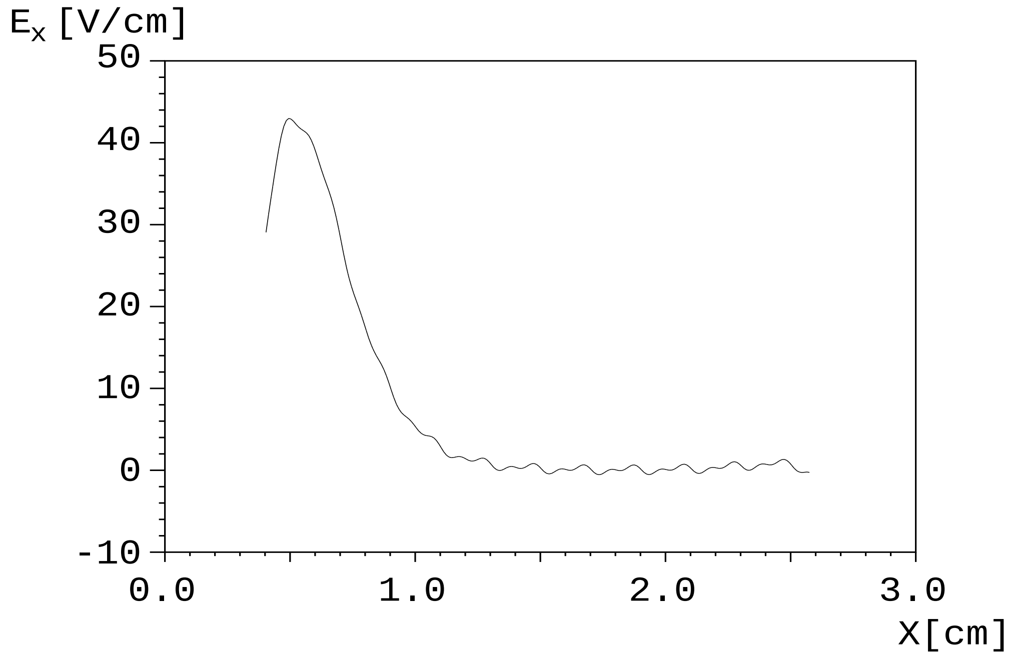

Figure 3.5: *Horizontal (X) component of the electric field between the gating grid and the Frisch grid in the readout region model. The cut is at R = 29.9 cm.*

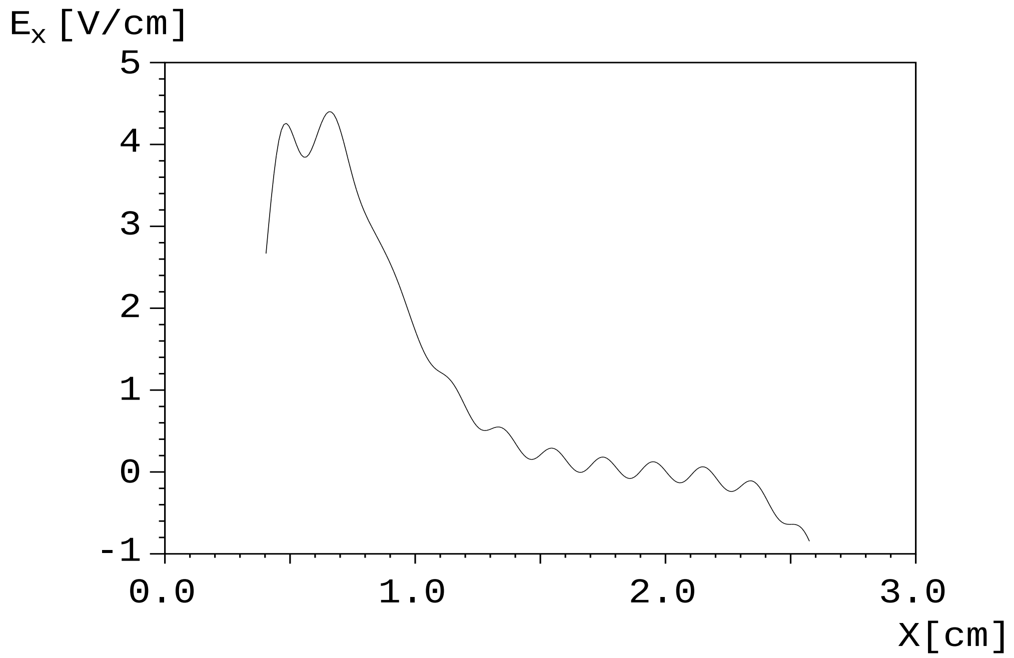

Figure 3.6: *Horizontal (X) component of the electric field in the drift volume below the gating grid. The cut is at R = 29.6 cm, 1.5 mm below the gating grid. The drop on the right results from the boundary conditions in the finite model.*

Chapter 4

Calculations for the Construction of the Field Cage

To estimate possible distortions of the main drift field caused by the field cage ring structure, a large-scale three-dimensional model of a complete FTPC was calculated using MAFIA. A visualization of the material distribution in the model can be seen in figure 4.1. All details of the readout sector structure have been neglected. The readout plane is modeled by a smooth surface on ground potential at the radius of the Frisch grid. The high voltage electrode is at a radius of 7.73 cm. The field cage rings at the two ends of the cylinder are modeled by solid, concentric structures at their actual positions. To test the separation of the drift field from possible disturbances outside the FTPC, two surfaces at ground potential were introduced. On one end of the FTPC, there is a narrow ring at small radius and a distance of 7 cm from the field cage, corresponding to the beam pipe connection of the inner FTPC insulation; on the other end, there is a solid plate at a distance of 10 cm from the field cage as a worst case for a possible disturbance. The field inside the sensitive volume of the chamber turned out to be almost completely insensitive against these disturbances.

Calculations were done using first the idealized radii and ring voltages. In further calculations, the voltages were set to the voltages actually achievable with the used divider chain, and the radii of individual field cage rings were varied according to realistic mechanical precision.

Field distortions were analyzed within the sensitive volume of the FTPC, the volume from where electrons can drift onto the pads and lead to a signal. This sensitive volume ends at a distance of more than 10 cm in z direction from the field cage. Therefore, the field in the sensitive volume is only weakly influenced by the field cage.

In the original FTPC design, the major source of distortions was the innermost field cage ring, which is mechanically and electrically connected to the high voltage electrode, as can be seen in figure 4.2. Therefore, its potential is several hundred Volts different from the ideal value, causing local distortions on the per mille level in the sensitive volume at small radii. The potential of the second field cage ring was adjusted for the best possible compensation, reducing the distortion by an order of magnitude. In the final FTPC design, the resistors in the divider chain defining the field cage potentials were changed accordingly.

The remaining distortions were calculated to be locally limited and smaller than one per mille of the drift field strength. They affect only the z component of the field (to which the detector resolution is mostly insensitive) and the radial component. The most critical coordinate for the performance of the detector is azimuthal. Significant azimuthal components in the drift field should only exist if the high voltage electrode or the field cage rings are not sufficiently circular or mounted off-center. Calculations were done assuming field cage rings that are off-center by reasonably pessimistic values, and the resulting azimuthal components were found to be negligible.

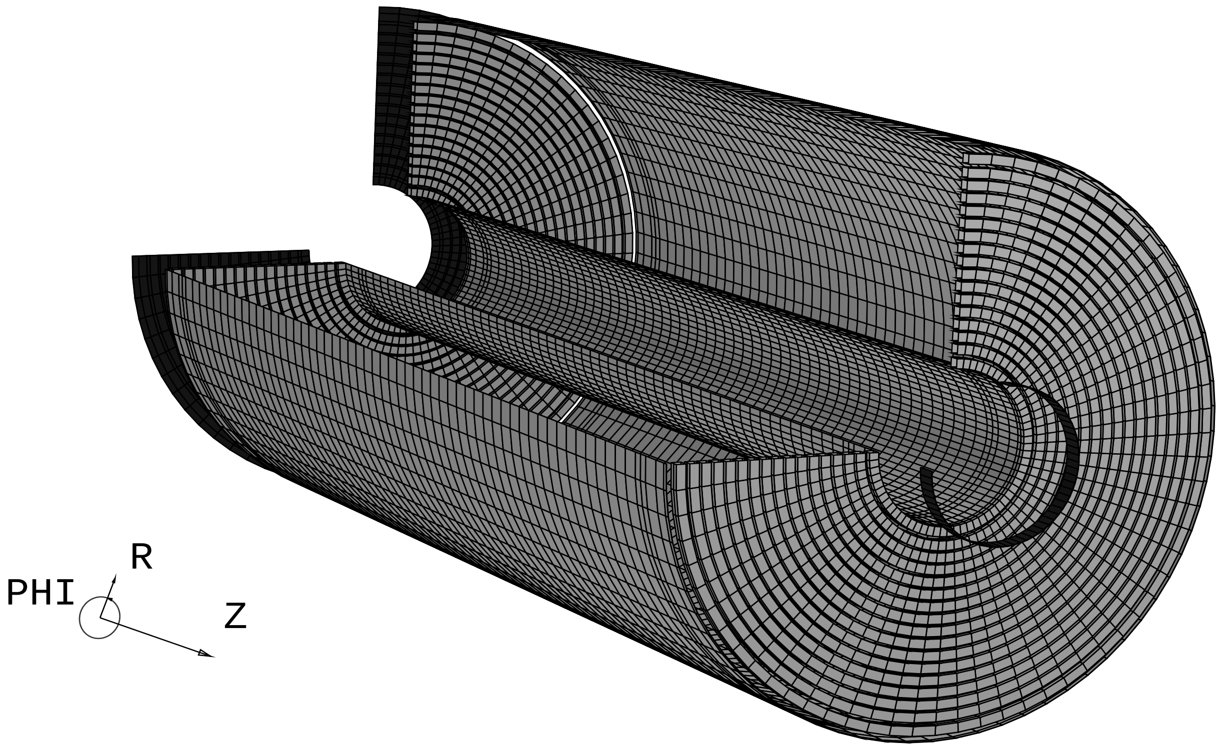

Figure 4.1: *Three dimensional view of the material distribution in the model to calculate the electrical drift field. Cylindrical coordinates are used to limit the complexity of the model, with the Z coordinate corresponding to z in the STAR coordinate system. The lightly shaded surfaces are the high voltage electrode, readout plane and field cage of the FTPC. Test surfaces at ground potential outside the FTPC are in a darker shade.*

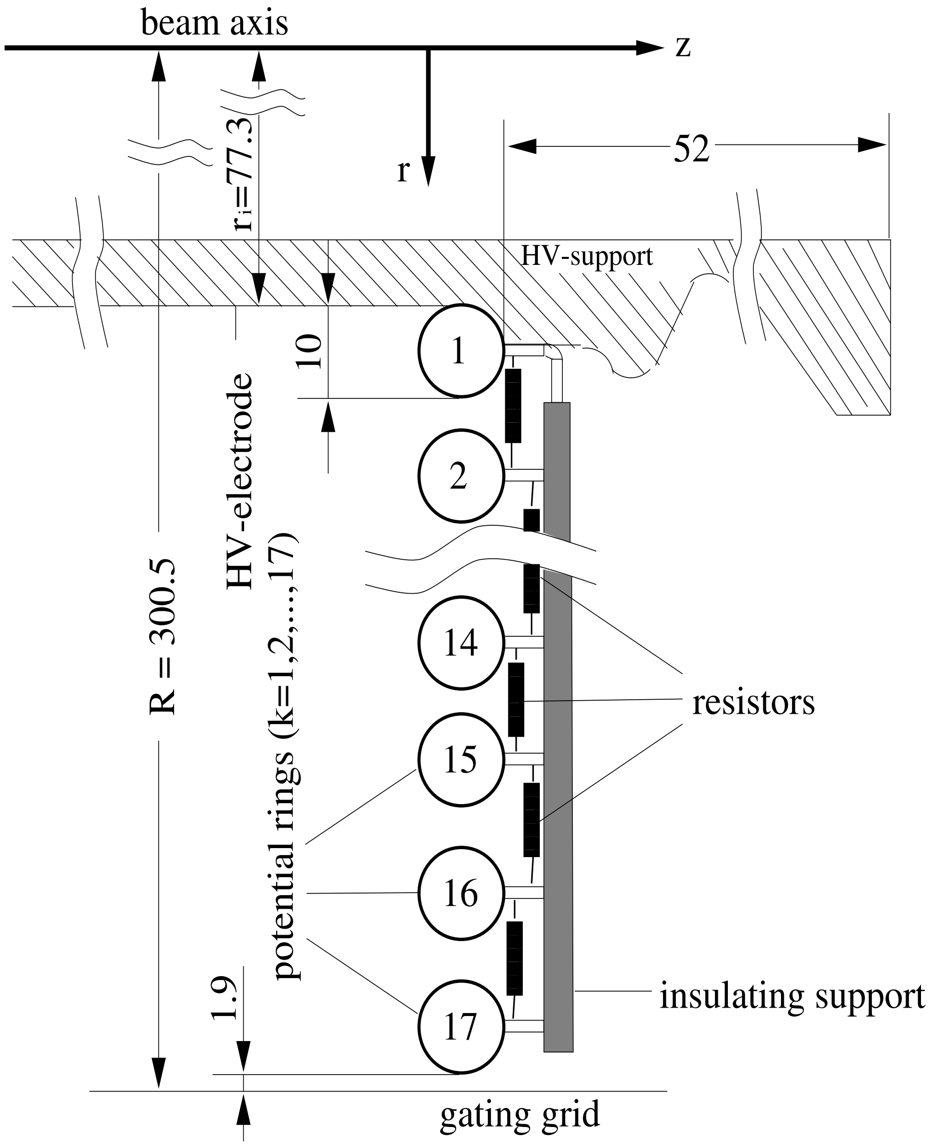

Figure 4.2: *Cut through the aluminum ring structure of the field cage, which separates the radial drift field from disturbances outside the chamber. The potential of the individual rings is defined by a resistor chain. The innermost ring touches the high voltage electrode and is therefore not at the potential corresponding to its radius. All lengths are in mm.*

List of Figures

1.1 FTPC design components 4

2.1 Laser scan with different anode wire angles 6
2.2 Determination of the angle between wires and pads 7

3.1 Material distribution in the readout region model 9
3.2 Electric potential distribution in the readout region model 10
3.3 Electric field around the gating grid 11
3.4 Electric field between Frisch grid and anode grid 12
3.5 Electric field between gating grid and Frisch grid 13
3.6 Electric field in the drift volume 13

4.1 Material distribution in the drift field model 15
4.2 Field cage structure 16

Bibliography

[Bar92] M. Bartsch *et al.*, "Solution of Maxwell's Equations", Computer Physics Communications 73 22-39 (1992)

[Bel99] R. Bell, "Kalibration einer Driftkammer mit Myonenstrahl", diploma thesis, Ruprecht-Karls-Universität Heidelberg (1999)

[Bie98] F. Bieser *et al.*, "The Forward Time Projection Chamber for the STAR Detector", MPI-PhE/98-3, Max-Planck-Institut für Physik, München (1998)

[Hum97] H. Hümmler, "Untersuchung des elektrischen und magnetischen Feldes in den NA49 TPCs mit Hilfe von Laserspuren", diploma thesis, Universität Frankfurt (1997)

[Kon95] M. Konrad, "Two Track Resolution in Longitudinal Direction in a TPC with Radial Drift Field", STAR Note 214, 15 June 1995

[Mar98] R. Marstaller, "Bau und Test einer hochauflösenden, gebogenen Proportionalkammer zum Auslesen einer Spurendriftkammer (TPC) mit radialem Driftfeld", diploma thesis, Technische Universität München (1998)

[Sch99] A. Schüttauf *et al.*, "A Forward TPC for STAR", Nuclear Physics A661 677c-680c (1999)